From a Model of Lossy Flared Pipes to a General Framework for Simulation of Waveguides

Rémi Mignot, Thomas Hélie, Denis Matignon

***Abstract*—This paper deals with the theory and application of waveguide modeling of lossy flared acoustic pipes, relying on the Webster-Lokshin equation. This model describes the propagation of longitudinal waves in axisymmetric acoustic pipes with a varying cross-section, visco-thermal losses at the walls, and without assuming planar waves or spherical waves. Solving this model for a piece of pipe leads to a two-port system made of four transfer functions which mimic the global acoustic effects. Moreover, introducing some relevant physical interpretations makes it possible to separate elementary effects due to the geometry of the piece of pipe (section, slope, and curvature) and isolate corresponding elementary transfer functions. From this decomposition a framework is obtained which allows to recover some digital waveguide models introduced earlier in the literature. This work contributes to the standardization of some different waveguide models, and brings a higher level of refinement that is visco-thermal losses combined with curvature effects.**

Pacs: 43.20.Mv, 43.75.Zz

I. Introduction

Whereas signal processing approaches describe sounds, physical modeling describes internal acoustic or mechanic phenomena of the modeled system. For sound synthesis (of musical instruments or speech production, for example), it faithfully reproduces the behavior of the system, especially during transient states. Moreover, parametric models allow to obtain new virtual systems and explore new sounds, together with physical validation. However, digital time simulations sometimes require intensive computation from computers. That is why special care must be taken on the algorithmic complexity to perform real-time sound synthesis.

The aim of the present work is to build the model and the simulation of a varying cross-section pipe using the standard "Digital Waveguide Network" approach (see eg. [1], [2]). With this technique, a whole virtual resonator is built by connecting several systems which mimic the acoustic of pieces of pipe. The difficulty and the novelty is to include subtle, though perceptible, phenomena due to visco-thermal losses at the wall and continuously varying cross-sections (see eg. [3], [4], [5], [6], [7], [8], [9]).

In [10], a resonator is represented by the connection of pieces of lossless cylinder to model vocal tract. For low-cost digital simulation, a scattering network (the *Kelly-Lochbaum* framework) is derived. This framework contains delays for wave propagation and coefficients for reflexion at junctions of cylinders. In [11], the *Kelly-Lochbaum* framework is derived for a refined model of connection of lossless cones (with continuity of radius at junctions). In [12] and [14], visco-thermal losses are taken into account for connections of cylinders and cones respectively. In [16], connection of lossy cones with discontinuity of section is considered. In [17] the same *Kelly-Lochbaum* framework is recovered by considering a more refined model of connection of lossy flared pipes, using the *Webster-Lokshin* equation. It is a 1D-acoustic model, which describes the propagation of longitudinal waves in axisymmetric acoustic pipes, involving visco-thermal losses at the wall and a varying cross-section.

In the present work, starting from the *Webster-Lokshin* model for a piece of pipe, solutions in terms of traveling waves lead to a new framework in which each effect of the geometry of the pipe can be isolated. In spite of the apparent complexity of this framework at first glance, all elements are already known and well understood. Thanks to the remarkable symmetry of this framework, connecting pieces of pipe with a particular order of discontinuity (of section, slope, or curvature) makes it possible to recover all the above-mentioned waveguide models (cf. eg. [10]-[18]).

This paper is organized as follows. In section II, the acoustic model is presented and the analytic solution for the acoustic pressure is given in the Laplace domain. Then, pieces of pipe are modeled, deriving two-port systems in admittance and impedance convention, and finally for traveling waves. In section III, a physically inspired decomposition of two-port systems is performed. It allows the isolation of the "elementary" acoustic effects of the pipe on traveling waves, according to the chosen acoustic model. Then, a general framework for simulation of digital waveguides is obtained. In section IV, connecting two-ports systems, the model of a whole pipe can be built with a refined model. Moreover this model allows to recover former models of waveguides (concatenation of cylinders or cones). In section V are briefly presented the building of the discrete-time system, and some comparisons of digital simulations. Finally, section VI concludes this paper and opens some perspectives.

II. Propagation in a lossy flared acoustic pipe

This section presents the *Webster-Lokshin* model of a pipe, from which scattering matrices and equivalent two-port systems are derived. Two-ports are input/output systems related to the standard acoustic state (acoustic pressure and volume flow) or to traveling waves.

Rémi Mignot and Thomas Hélie are with IRCAM & CNRS, UMR 9912, 1, place Igor Stravinsky, 75004 Paris, France
Denis Matignon is with Université de Toulouse; ISAE, Applied Mathematics Training Unit, 10, av. E. Belin, 31055 Toulouse Cedex 4, France
Rémi Mignot is Ph.D. student at Télécom ParisTech/TSI
This work is supported by the CONSONNES project, ANR-05-BLAN-0097-01

A. Webster-Lokshin model

1) Equations for acoustic pressure and volume flow: The *Webster-Lokshin* model is a mono-dimensional model, which characterizes linear longitudinal waves propagation in axisymmetric pipes, assuming the quasi-sphericity of isobars near the inner wall (cf. [8], [19]), and taking into account visco-thermal losses (cf. [5], [3], [4]) at the wall. The acoustic pressure P and the volume flow U are governed by the following equations, given in the Laplace domain:

$$\left(\left[\left(\frac{s}{\mathrm{c}_0}\right)^2+2\,\varepsilon(\ell)\left(\frac{s}{\mathrm{c}_0}\right)^{\frac{3}{2}}+\Upsilon(\ell)\right]-\partial_\ell^2\right)\Big\{r(\ell)P(\ell,s)\Big\} \;=\; 0, \quad (1)$$

$$\rho_0\; s\,\frac{U(\ell,s)}{\mathrm{A}(\ell)}+\partial_\ell P(\ell,s) \;=\; 0, \quad (2)$$

where $s\in\mathbb{C}$ is the Laplace variable ($\Im\mathrm{m}(s)=\omega$ is the angular frequency), ℓ is the space variable measuring the arclength of the wall, $r(\ell)$ is the radius of the pipe, $\mathrm{A}(\ell):=\pi r(\ell)^2$ is the section area, $\varepsilon(\ell):=\kappa_0\sqrt{1-r'(\ell)^2}/r(\ell)$ quantifies the visco-thermal losses and $\Upsilon(\ell):=r''(\ell)/r(\ell)$ denotes the curvature of the wall. Equation (1) is called *Webster-Lokshin* equation, and (2) is *Euler* equation satisfied outside the visco-thermal boundary layer.

Note that the standard horn equation (cf. [6]) corresponds to (1) with no losses ($\varepsilon(\ell)=0$) and assuming planar waves (ℓ is replaced by the axis coordinate z). Straight and conical pipes are characterized by $\Upsilon(\ell)=0$. In the following, Υ is assumed to be non-negative, corresponding to straight, conical or flared pipes. The negative case would require special treatments for deriving stable versions of waveguides (cf. [7]), which are out of the scope of this paper.

Denoting $\underline{r}(z)$ the radius of the pipe for the z-ordinate, the arclength of the wall from 0 to z is

$$\ell(z)=\int_0^z\sqrt{1+\underline{r}'(z)^2}\;\mathrm{d}z \quad (3)$$

and $\underline{r}(z):=r(\ell(z))$. In consequence, $|r'(\ell)|<1$ and $r'(\ell)\to 1$ when $\underline{r}'(z)\to+\infty$.

For numerical computations, the physical constants are chosen for standard conditions. They are: the mass density $\rho_0=1.2$ kg.m^{-3}, the speed of sound $\mathrm{c}_0=344$ m.s^{-1}, the coefficient $\kappa_0=\sqrt{l_v'}+(\gamma-1)\sqrt{l_h}\approx 3.5\;10^{-4}$ m$^{-\frac{1}{2}}$.

2) Limitations of the model: The *Webster-Lokshin* model only considers axisymmetric pipes. Consequently, the possible bends (of a trombone slide for example) have to be virtually straightened. Moreover, two other limitations appear because of the visco-thermal losses model and because only longitudinal propagations are considered.

With l_v' and l_h the characteristic lengths of viscous ($l_v'\approx 4\,10^{-8}$m) and thermal ($l_h\approx 6\,10^{-8}$m) effects (cf. [20]), this model of losses is valid for "large tubes" given by $r\gg\sqrt{2\mathrm{c}_0 l_v'/\omega}$ and $r\gg\sqrt{2\mathrm{c}_0 l_h/\omega}$. For example, with $r=5$ mm, the model is valid for $f=\omega/(2\pi)\gg 0.25$ Hz.

For a lossless cylinder with radius r, the first transversal mode appears at $f=1.84\,\mathrm{c}_0/(2\pi r)$. In the case of a varying cross-section pipe, transversal modes appear with frequencies higher than $1.84\,\mathrm{c}_0/(2\pi r_m)$, where r_m is the maximal radius of the pipe. For example, with $r_m=10$ cm, the *Webster* model remains valid for $f<1000$ Hz. Note that, multi-modal approaches allow to simulate transversal modes (cf. eg. [21]).

3) Equations for traveling waves: In sec. II-A1 the acoustic pressure $P(\ell,s)$ and volume flow $U(\ell,s)$ are used to describe acoustics. Another description, more adapted to the waveguide simulations, consists in using the traveling waves defined by:

$$\begin{bmatrix}\phi^+(\ell,s)\\ \phi^-(\ell,s)\end{bmatrix} \;:=\; \frac{r(\ell)}{2}\begin{bmatrix}1 & Z(\ell)\\ 1 & -Z(\ell)\end{bmatrix}\begin{bmatrix}P(\ell,s)\\ U(\ell,s)\end{bmatrix}, \quad (4)$$

where $Z(\ell):=1/Y(\ell):=\rho_0\,\mathrm{c}_0\,/\,\mathrm{A}(\ell)$ is the equivalent of acoustic impedance for planar waves traveling inside cylinder of (constant) section area $\mathrm{A}=\mathrm{A}(\ell)$.

According to (1), (2) and (4), these traveling waves are governed by the coupled system

$$\left(\frac{s}{c_0}\pm\partial_\ell\right)\phi^{\mp}(\ell,s)=\pm\zeta(\ell)\phi^{\mp}(\ell,s)-\varepsilon(\ell)\left(\frac{s}{c_0}\right)^{\frac{1}{2}}\phi(\ell,s), \quad (5)$$

where $\phi:=\phi^+-\phi^-=rP$, and $\zeta:=r'/r$. The operator $\left(s/\mathrm{c}_0\pm\partial_\ell\right)$ is the traveling operator and the right-hand side describes the coupling due to $\zeta(\ell)$ and losses.

For planar waves traveling inside a lossless straight pipe ($\varepsilon(\ell)=0$ and $\zeta(\ell)=0$), the acoustic state $\phi^{\pm}$ corresponds to decoupled progressive waves. For the Wester-Lokshin model, these waves are still progressive insofar as they preserve the causality principle.

B. Piece of pipe and general solution

In this paper, a pipe with varying cross-section is approximated by a concatenation of pieces of pipe with constant parameters. So, a piece of pipe is defined as a finite pipe with length L, and with constant curvature and losses parameters (i.e $\Upsilon(\ell)=\Upsilon$ and $\varepsilon(\ell)=\varepsilon$). This allows to preserve the continuity of radius $r(\ell)$ and slope $r'(\ell)$ that is $\mathcal{C}^1$-regular shapes. Junctions are characterized by discontinuities of curvature.

Remark that, except for a cylinder, $\Upsilon(\ell)$ and $\varepsilon(\ell)$ cannot be simultaneously constant. In pratice, pieces of pipe with constant curvature are considered, and ε is chosen as the mean of $\varepsilon(\ell)$. This approximation makes sense, at least for physically realistic lengths and curvatures for wind instruments.

In a such piece of pipe (Υ and ε contant), the general solution of the acoustic pressure $P(\ell,s)$ for (1) is:

$$P(\ell,s)=\mathcal{A}(s)\frac{\mathrm{e}^{\Gamma(s)\ell}}{r(\ell)}+\mathcal{B}(s)\frac{\mathrm{e}^{-\Gamma(s)\ell}}{r(\ell)}, \quad (6)$$

where $\mathcal{A}(s)$ and $\mathcal{B}(s)$ depend on boundary conditions, and $\Gamma(i\omega)=ik(\omega)$ for which $k(\omega)$ is the usual complex wavenumber. Γ is given in the Laplace domain by:

$$\Gamma(s)=\sqrt{\left(\frac{s}{\mathrm{c}_0}\right)^2+2\,\varepsilon\left(\frac{s}{\mathrm{c}_0}\right)^{\frac{3}{2}}+\Upsilon}. \quad (7)$$

In (7) $\sqrt{.}$ denotes an analytical continuation of the positive square root of $\mathbb{R}^+$ on a domain compatible with the one-sided Laplace transform, namely $\mathbb{C}_0^+=\{s\in\mathbb{C}/\Re e(s)>0\}$ (see [9] for more details). In $\mathbb{C}_0^+$, Γ is proved to be analytical and $\Re e(\Gamma(s))\geq 0$ if $\varepsilon\geq 0$.

If $\Upsilon\geq 0$ and $\varepsilon=0$, the unique positive solution $\omega_c=\sqrt{\Upsilon}/\,\mathrm{c}_0$ of $\Gamma(i\omega)^2=0$, corresponds to the cutoff angular

frequency of a lossless pipe with positive constant curvature. Indeed, if $\omega > \omega_c$, $\Gamma(i\omega) \in i\mathbb{R}$, it corresponds to propagating waves, and if ω is such that $0 \leq \omega < \omega_c$, $\Gamma(i\omega) \in \mathbb{R}^+$, it corresponds to evanescent waves.

Now, if $\Upsilon \geq 0$ and $\varepsilon > 0$, a similar behavior is obtained for $\omega_c = \Im m(s_c) > 0$ where $(s_c, \overline{s_c})$ are the unique solutions of $\Gamma(s)^2 = 0$; they satisfy $\Re e(s_c) < 0$ (cf. [9]).

More details of the effects of visco-thermal losses and curvature on transfer functions are given in appendix C.

C. Scattering matrices and equivalent two-port systems

In the following, P_0 and P_L are defined as the acoustic pressure at the left end ($\ell = 0$) and at the right end ($\ell = L$) of a piece of pipe with $\Upsilon(\ell) = \Upsilon$ and $\varepsilon(\ell) = \varepsilon$. In the same way U_0, U_L, are defined as the volume flow at the left and the right ends, respectively.

1) Scattering matrix with admittance representation: Writing $[U_0,\, U_L]$ as functions of $[P_0,\, P_L]$, the piece of pipe is modeled by the 2×2 scattering matrix $\mathcal{H}(s)$. Figure 1 represents the corresponding two-port system $\mathbf{Q}_{PU}$.

$$\begin{bmatrix} U_0 \\ U_L \end{bmatrix} = \mathcal{H} \begin{bmatrix} P_0 \\ P_L \end{bmatrix} = \begin{bmatrix} H_{11} & H_{12} \\ H_{21} & H_{22} \end{bmatrix} \begin{bmatrix} P_0 \\ P_L \end{bmatrix}. \tag{8}$$

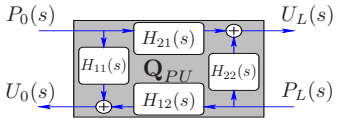

Fig. 1. Two-port system $\mathbf{Q}_{PU}$, with admittance representation.

Solving (1) and (2) leads to the following closed forms of elements of $\mathcal{H}$ (cf. [19]):

$$H_{11}(s) = \frac{\mathrm{A}_l}{\rho_0} \frac{\Gamma(s)\,\cosh(\,\Gamma(s)L\,) + \zeta_l \sinh(\,\Gamma(s)L\,)}{s\sinh(\,\Gamma(s)L\,)}, \tag{9}$$

$$H_{22}(s) = \frac{\mathrm{A}_r}{\rho_0} \frac{\Gamma(s)\,\cosh(\,\Gamma(s)L\,) - \zeta_r \sinh(\,\Gamma(s)L\,)}{s\sinh(\,\Gamma(s)L\,)}, \tag{10}$$

$$H_{12}(s) = -\frac{r_l}{r_r}\frac{\mathrm{A}_l}{\rho_0} \frac{\Gamma(s)}{s\sinh(\,\Gamma(s)L\,)}, \tag{11}$$

$$H_{21}(s) = -\frac{r_r}{r_l}\frac{\mathrm{A}_r}{\rho_0} \frac{\Gamma(s)}{s\,\sinh(\,\Gamma(s)L\,)}, \tag{12}$$

where $\Gamma(s)$ is defined by (7), and the following notations are introduced (with indexes $i = l$ and $i = r$, which mean *left* and *right*): $r_i = r(\ell_i)$ (radius), $\mathrm{A}_i = \pi r_i^2$ (section area), $r_i' = r'(\ell_i)$ (slope), $\zeta_i = r_i'/r_i$, with $\ell_l = 0$ and $\ell_r = L$.

Remark: If $P_L(s) = 0$, equation (8) gives $U_0 = H_{11}P_0$. Hence, H_{11} can be interpreted as the left input admittance of a lossy flared pipe with constant curvature which is ideally open at the right end. Conversely, the impedance of such a pipe is given by $1/H_{11}(s)$ (cf. Fig. 2). Its comparisons for some values of Υ are given in appendix C.

2) Scattering matrix with impedance representation: Similarly to sec. II-C1, now the piece of pipe is modeled by the scattering matrix $\mathcal{G}(s)$ where $[U_0(s), U_L(s)]^T$ is the input and $[P_0(s), P_L(s)]^T$ is the output.

$$\begin{bmatrix} P_0 \\ P_L \end{bmatrix} = \mathcal{G} \begin{bmatrix} U_0 \\ U_L \end{bmatrix} = \begin{bmatrix} G_{11} & G_{12} \\ G_{21} & G_{22} \end{bmatrix} \begin{bmatrix} U_0 \\ U_L \end{bmatrix}. \tag{13}$$

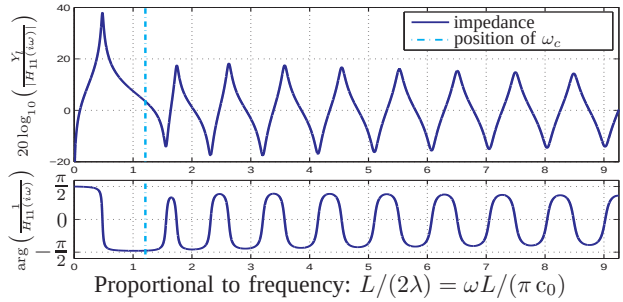

Fig. 2. Impedance of open piece of pipe, H_{11}^{-1}. $r_l = 5$ mm, $r_r = 1$ cm, $L = 1$ m, $\Upsilon = 15$ m^{-2}. $Y_l = \mathrm{A}_l/(\rho_0\,\mathrm{c}_0)$.

It results in the following relation between the scattering matrices: $\mathcal{G} = \mathcal{H}^{-1}$. The corresponding two-port system (not represented) is named $\mathbf{Q}_{UP}$.

Remark: $U_L(s) = 0$ leads to $P_0 = G_{11}U_0$, so that G_{11} can be interpreted as the left input impedance of a closed lossy flared pipe with constant curvature (cf. Fig. 3).

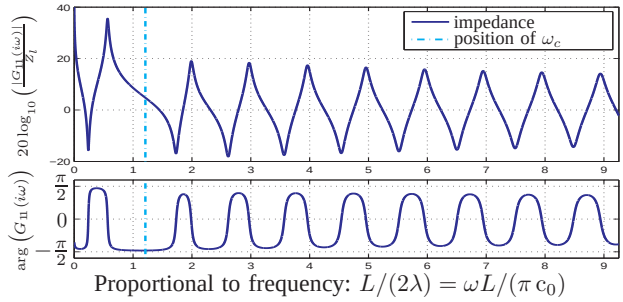

Fig. 3. Impedance of closed piece of pipe, G_{11}. $r_l = 5$ mm, $r_r = 1$ cm, $L = 1$ m, $\Upsilon = 15$ m^{-2}. $Y_c = \mathrm{A}_l/(\rho_0\,\mathrm{c}_0)$.

3) Scattering matrix for the traveling waves (ϕ^+, ϕ^-): Now traveling waves $\phi^\pm$ defined by (4) are considered. The piece of pipe is modeled by a system, where inputs are $\phi_0^+(s) := \phi^+(\ell = 0, s)$ and $\phi_L^-(s) := \phi^-(\ell = L, s)$ (incoming waves at $\ell = 0$ and $\ell = L$), and outputs are $\phi_0^-(s)$ and $\phi_L^+(s)$ (outgoing waves).

This system is represented by the scattering matrix $\mathcal{M}_\phi$ and the two-port $\mathbf{Q}_\phi$ of Fig. 4.

$$\begin{bmatrix} \phi_0^- \\ \phi_L^+ \end{bmatrix} = \mathcal{M}_\phi \begin{bmatrix} \phi_0^+ \\ \phi_L^- \end{bmatrix} = \begin{bmatrix} R_g^l & T_g^- \\ T_g^+ & R_g^r \end{bmatrix} \begin{bmatrix} \phi_0^+ \\ \phi_L^- \end{bmatrix}. \tag{14}$$

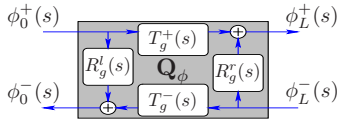

Fig. 4. Two-port $\mathbf{Q}_\phi$, with traveling waves.

The closed form expressions of elements of $\mathcal{M}_\phi$ are not detailed in this paper, but can be found eg. in [19].

Remark: Transfer functions R_g^l and R_g^r represent left (index *l*) and right (index *r*) *global* (index *g*) reflexions of the pipe (with length L) on traveling waves. "Global" means that every internal effects of the pipe are mixed in these transfer functions. An analysis of internal effects is detailed in sec. III.

T_g^+ and T_g^- represent global transmissions of traveling waves through the pipe.

4) Conversion two-port systems: The three different two-ports represented in sections II-C1, II-C2 and II-C3 can be intertwined using conversion two-ports given in Fig. 5, which are deduced from (4). These conversion two-ports are denoted $\mathcal{C}_{a,b}$, where a is the left acoustic state (PU, UP or ϕ) and b is the right state.

For example to deduce the two-port $\mathbf{Q}_\phi$ from $\mathbf{Q}_{PU}$, the two-port $\mathcal{C}_{\phi,PU}$ has to be connected on the left side of $\mathbf{Q}_{PU}$ and $\mathcal{C}_{UP,\phi}$ on the right side.

That means: $\mathbf{Q}_\phi \equiv \mathcal{C}_{\phi,PU} \odot \mathbf{Q}_{PU} \odot \mathcal{C}_{UP,\phi}$, where $\equiv$ is the equivalent relation and $\odot$ is the connection operator. See appendix A where global interconnection laws of 2 two-ports are given, or see [22] for a state-space representation.

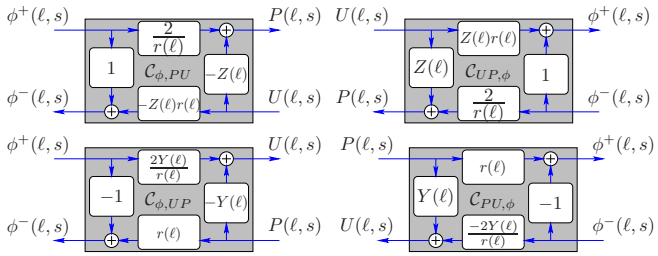

Fig. 5. Conversion two-ports $\mathcal{C}_{\phi,PU}$, $\mathcal{C}_{UP,\phi}$, $\mathcal{C}_{\phi,UP}$ and $\mathcal{C}_{PU,\phi}$.

III. Physically inspired decomposition of the two-port

The scattering matrices $\mathcal{H}$, $\mathcal{G}$ and $\mathcal{M}_\phi$ derived from the *Webster-Lokshin* model characterize the global acoustic behavior of a piece of pipe. In this section, their decomposition into elementary two-port systems is performed. First, delays $\mathrm{e}^{-i\omega L/\,\mathrm{c}_0}$ representing an ideal propagation are isolated from other operators without internal delays. Second, in the latter operators, effects of the shape due to radius, slope and curvature can be isolated ones from the other. These decompositions are not purely algebraic manipulations: they rely on physically based reasoning and yield straightforward interpretations. Moreover, they will allow to improve the corresponding digital waveguide implementation.

A. Separating delays and acoustic effects

Defining

$$T(s) := \mathrm{e}^{-\Gamma(s)L} = D(s)\,\mathrm{e}^{-s\frac{L}{\mathrm{c}_0}}, \tag{15}$$

$$\text{with}\quad D(s) := \mathrm{e}^{-\left(\Gamma(s)-\frac{s}{\mathrm{c}_0}\right)L}, \tag{16}$$

in [9], $D(s)$ is proved to be causal and stable, so that $T(s)$ represents the delay ($\mathrm{e}^{-i\omega L/\mathrm{c}_0}$) of the wave propagation through the piece of pipe, and the associated effect ($D(s)$) due to curvature and visco-themal losses.

This section is dedicated to isolate pure delay operators which are contained in $T(s) = \mathrm{e}^{-\Gamma(s)L}$ and to deduce a framework which isolates them.

1) Decomposition of $\mathbf{Q}_\phi$: In Fig. 4, the transfer functions R_g^l, R_g^r, T_g^+ and T_g^+ represent global effects of a piece of pipe on the traveling waves $\phi^\pm$. Nevertheless, some elementary effects can be isolated using the following relevant interpretations (see Fig. 6): At the left end ($\ell = 0$), the incident wave ϕ_0^+ is partially reflected in the opposite direction (modeled in Fig. 6 by the transfer function R_{le}) and is partially transmitted into the piece of pipe (T_{le}). Then, this transmitted part travels inside the pipe until the right end located at $\ell = L$ (T^+), before being partially reflected (R_{ri}) and partially transmitted (T_{ri}) outside the pipe. Symmetrically, the incident wave ϕ_L^- undergoes similar phenomena.

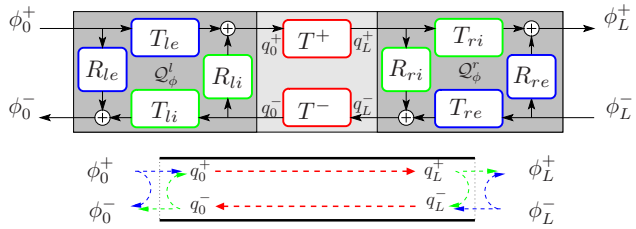

Fig. 6. Decomposition of the two-port $\mathbf{Q}_\phi$.

Figure 6 compiles these phenomena and includes all the contributions (the indexes i and e mean *internal* and *external*, respectively; the functions T^+ and T^- represent the forward and backward transmissions through the pipe, respectively).

This decomposition enlights two smaller two-port systems, $\mathcal{Q}_\phi^l$ and $\mathcal{Q}_\phi^r$ (cf. Fig. 6), which models left and right semi-interfaces, respectively.

The two-ports described in Fig. 4 and Fig. 6 are equivalent if the following algebraic equations hold:

$$T_g^+ = \frac{T_{le}\,T_{ri}\,T^+}{1 - R_{ri}\,R_{li}\,T^-\,T^+}, \tag{17}$$

$$T_g^- = \frac{T_{re}\,T_{li}\,T^-}{1 - R_{ri}\,R_{li}\,T^-\,T^+}, \tag{18}$$

$$R_g^l = R_{le} + \frac{R_{ri}\,T_{le}\,T_{li}\,T^+\,T^-}{1 - R_{ri}\,R_{li}\,T^-\,T^+}, \tag{19}$$

$$R_g^r = R_{re} + \frac{R_{li}\,T_{re}\,T_{ri}\,T^+\,T^-}{1 - R_{ri}\,R_{li}\,T^-\,T^+}. \tag{20}$$

Equations (17-20) do not lead to a unique identification of (T_{li}, R_{li}, T_{le}, R_{le}, T^+, T^-, T_{ri}, R_{ri}, T_{re}, R_{re}) from (R_g^l, R_g^r, T_g^+ and T_g^-). Nevertheless, the following hypotheses with good sense yield a unique identification:

(H1) Pressure continuity $\phi_l^+ + \phi_l^- = q_l^+ + q_l^-$ for $l \in \{0, L\}$ is required (see Fig. 6). This hypothesis implies that *every reflection r and every transmission t fed by the same input are such that $t = 1 + r$.*

(H2) The left-hand side functions (of $\mathcal{Q}_\phi^l$) depend only on the *left parameter* ζ_l. Respectively, the right-hand side functions (of $\mathcal{Q}_\phi^r$) depend on the *right parameter* ζ_r.

(H3) The propagation transfer functions $T^\pm$ include a pure delay operator: $T^\pm(s) = D^\pm(s)\,\mathrm{e}^{-sL/\mathrm{c}_0}$, where $D^\pm(s)$ are causal and stable.

Then, the unique solution is proved to be (cf. [17])

$$T^+(s) = T^-(s) = T(s) = \mathrm{e}^{-\Gamma(s)L}, \quad (21)$$

$$R_{re}(s) = -\frac{\Gamma(s) - \frac{s}{c_0} - \zeta_L}{\Gamma(s) + \frac{s}{c_0} - \zeta_L} = 1 - T_{re}(s), \quad (22)$$

$$R_{le}(s) = -\frac{\Gamma(s) - \frac{s}{c_0} + \zeta_0}{\Gamma(s) + \frac{s}{c_0} + \zeta_0} = 1 - T_{le}(s), \quad (23)$$

$$R_{ri}(s) = \frac{\Gamma(s) - \frac{s}{c_0} + \zeta_L}{\Gamma(s) + \frac{s}{c_0} - \zeta_L} = 1 - T_{ri}(s), \quad (24)$$

$$R_{li}(s) = \frac{\Gamma(s) - \frac{s}{c_0} - \zeta_0}{\Gamma(s) + \frac{s}{c_0} + \zeta_0} = 1 - T_{li}(s). \quad (25)$$

2) Decomposition of $\mathbf{Q}_{PU}$ and $\mathbf{Q}_{UP}$: A similar decomposition of two-ports with acoustic state (P, U) is obtained in Fig. 7. For instance, $\mathcal{Q}^l_{PU}$ is obtained by connecting $\mathcal{C}_{PU,\phi}$ with $\mathcal{Q}^l_\phi$ (which means $\mathcal{Q}^l_{PU} \equiv \mathcal{C}_{PU,\phi} \odot \mathcal{Q}^l_\phi$), following the process detailed in sec. A.

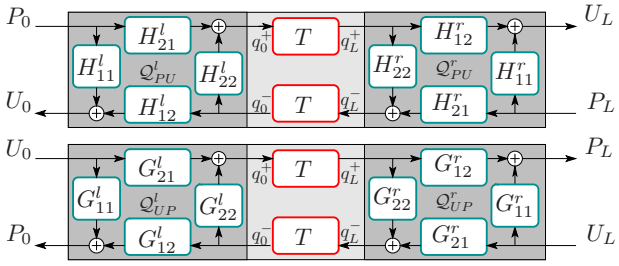

Fig. 7. Decomposition of the two-port $\mathbf{Q}_{PU}$ and $\mathbf{Q}_{UP}$.

Transfer functions H^x_{ij} and G^x_{ij} of Fig. 7 (with $x \in \{l, r\}$) are rational functions of s and $\Gamma(s)$.

Note that two-ports $\mathbf{Q}^l_{PU}$, $\mathbf{Q}^r_{PU}$, $\mathbf{Q}^l_{UP}$ and $\mathbf{Q}^r_{UP}$, of Fig. 7, can be interpreted as conversion two-ports to new variables, $q^+(\ell, s)$ and $q^-(\ell, s)$, which are decoupled.

Remark: Since $\Re e(\Gamma(s)) > 0$, for all $s \in \mathbb{C}$ such that $\Re e(s) \geq 0$ (see [9]), then

$$T(s) = \mathrm{e}^{-\Gamma(s)L} \to 0 \text{ when } L \to +\infty. \quad (26)$$

Consequently $P_0(s) \approx G^l_{11}(s) U_0(s)$ (when $L \to \infty$), and the transfer function G^l_{11} is interpreted as the left input impedance of a lossy semi-infinite pipe with constant curvature (cf. Fig. 8). H^l_{11} is its corresponding admittance. The expressions of G^l_{11} and H^l_{11} are

$$G^l_{11}(s) = \frac{1}{H^l_{11}(s)} = \frac{Z_l}{\mathrm{c}_0} \frac{s}{\Gamma(s) + \zeta_l}. \quad (27)$$

B. Separating effects of pipe geometry

This section now focuses on separating contributions on the acoustics due to the radius r, the slope r' and the curvature r''/r, and their possible discontinuities. The different orders of discontinuity of the shape are introduced:

- The 0-*order* corresponds to a discontinuity of radius r at junctions,
- The 1-*order* corresponds to a discontinuity of slope r',
- The 2-*order* corresponds to a discontinuity of curvature $\Upsilon = r''/r$.

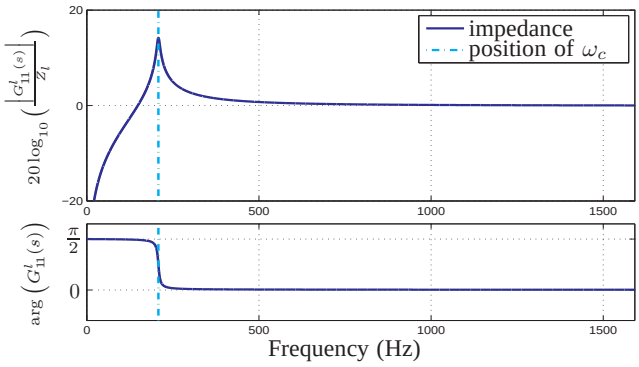

Fig. 8. Impedance of semi-infinite piece of pipe, $G^l_{11}(s = 2i\pi f)$ for $r_l = 5$ mm, $\Upsilon = 15\ \mathrm{m}^{-2}$, $\varepsilon = 0.0525\ \mathrm{m}^{-\frac{1}{2}}$, $\zeta_l = 0\ \mathrm{m}^{-1}$.

Contrarily to connections of straight or conical pipes, the *Webster-Lokshin* model enables connections of pipes preserving $\mathcal{C}^1$-regularity, which means the continuity of section and slope, and discontinuity of curvature (2-order of discontinuity).

1) Change of variables at interfaces of pipe: In order not to "hide" some effects of the geometry of the piece of pipe inside conversion two-ports, it is useful to define a change of variables independent from the pipe under interest. Thus, a *reference pipe* is introduced, which is a lossless cylinder with radius r_c, and defined variables correspond to planar traveling waves for this reference pipe. Its characteristic impedance is $Z_c = 1/Y_c = \rho_0\, \mathrm{c}_0 \,/\, \mathrm{A}_c$ (with $\mathrm{A}_c = \pi r_c^2$), and planar traveling waves are, for $\ell \in \{0, L\}$:

$$\begin{bmatrix} p^+(\ell, s) \\ p^-(\ell, s) \end{bmatrix} = \frac{1}{2} \begin{bmatrix} 1 & Z_c \\ 1 & -Z_c \end{bmatrix} \begin{bmatrix} P(\ell, s) \\ U(\ell, s) \end{bmatrix}. \quad (28)$$

For lossy varying cross-section pipes, (p^+, p^-) are neither decoupled nor perfectly progressive inside the pipe. Nethertheless, they keep "physical meaning" at interfaces of pipe, as the decomposition detailed below enlights.

In sec. IV-B will be shown that variables $p^\pm$ disappear after connection of two pieces of pipe, so that the value of r_c (or Z_c) is arbitrary and does not affect the modeling.

2) Decomposed framework: Figure 9 presents the framework where effects of geometry are separated into some two-ports: two-ports $\mathcal{Q}^l_a$ and $\mathcal{Q}^r_a$ for the effects of section at left and right ends respectively, $\mathcal{Q}^l_s$ and $\mathcal{Q}^r_s$ for slope, $\mathcal{Q}^l_{cl}$ and $\mathcal{Q}^r_{cl}$ for curvature.

With $\mathcal{C}'_{PU,p}$ the conversion two-port from (P, U) to $p^\pm$ and $\mathcal{C}'_{p,UP}$ its reciprocal conversion, this framework proves to be equivalent to $\mathbf{Q}_{PU}$ (see sec. II-C1). The proof uses interconnection laws of two-port systems (see appendix A).

Note that this framework naturally enlights 4 consecutive change of variables:

$p^\pm$: variables defined by (28),
$\phi^\pm$: traveling waves defined by (4),
$\psi^\pm$: symmetrical traveling waves defined in [9],
$q^\pm$: decoupled variables.

The remarkable thing of the framework of Fig. 9, is that it isolates a central part for wave propagation and 6 cells of the *Kelly-Lochbaum* junction type (cf. [10]), of which 4 are well-known (effects of section and slope) and 2 are new as far as we know.

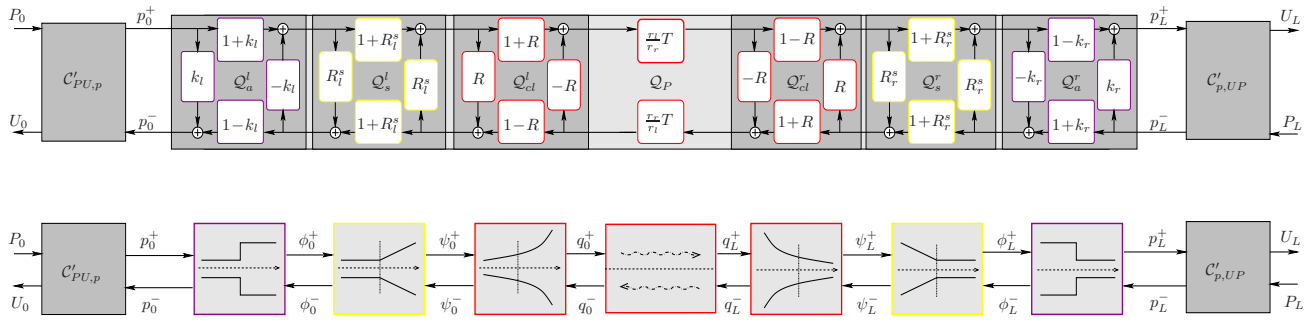

Fig. 9. Decomposed framework, where effects of the pipe geometry are separated.

3) Interpretation of cells:

- *Cells $\mathcal{Q}_a^l$ and $\mathcal{Q}_a^r$*
  $\mathcal{Q}_a^l$ and $\mathcal{Q}_a^r$, with coefficients k_l and k_r, take into account sections of pipe $\mathrm{A}_l = \pi r_l^2$ and $\mathrm{A}_r = \pi r_r^2$, at ends. The index "**a**" means "**a**rea of section". They are similar to cells of the *Kelly-Lochbaum* framework after connection with a lossless cylinder of radius r_c (cf. eg. [10], [13]).

$$k_l = \frac{\mathrm{A}_c - \mathrm{A}_l}{\mathrm{A}_c + \mathrm{A}_l} = -\frac{Z_c - Z_l}{Z_c + Z_l}, \tag{29}$$

$$k_r = \frac{\mathrm{A}_c - \mathrm{A}_r}{\mathrm{A}_c + \mathrm{A}_r} = -\frac{Z_c - Z_r}{Z_c + Z_r}. \tag{30}$$

- *Cells $\mathcal{Q}_s^l$ and $\mathcal{Q}_s^r$*
  $\mathcal{Q}_s^l$ and $\mathcal{Q}_s^r$, with transfer functions R_l^s and R_r^s, take into account slopes of pipe $r_l' = r'(\ell = 0)$ and $r_r' = r'(\ell = L)$ at left and right sides. The index "**s**" means "**s**lope". They are similar to cells of the framework of *Kelly-Lochbaum* after connection of cones (cf. eg. [11], [14]).

$$R_l^s(s) = \frac{\alpha_l}{s - \alpha_l}, \quad \text{with } \alpha_l = -\frac{\mathrm{c}_0}{2}\frac{r_l'}{r_l}, \tag{31}$$

$$R_r^s(s) = \frac{\alpha_r}{s - \alpha_r}, \quad \text{with } \alpha_r = +\frac{\mathrm{c}_0}{2}\frac{r_r'}{r_r}. \tag{32}$$

  If the slope is 0 (for cylinders for instance), these cells become identity ($\phi_\ell^\pm = \psi_\ell^\pm$).
- *Cells $\mathcal{Q}_{cl}^l$ and $\mathcal{Q}_{cl}^r$*
  $\mathcal{Q}_{cl}^l$ and $\mathcal{Q}_{cl}^r$, with the transfer function R, take into account the constant curvature and losses of the pipe. The indexes "**cl**" means "**c**urvature and **l**osses".

$$R(s) = \frac{\dfrac{s}{\mathrm{c}_0} - \Gamma(s)}{\dfrac{s}{\mathrm{c}_0} + \Gamma(s)}. \tag{33}$$

  In the case of lossless cones or cylinders ($\Upsilon = \varepsilon = 0$), $R = 0$, thus these cells are identity ($\psi_\ell^\pm = q_\ell^\pm$).

Using (26), in [23], the transfer function $R(s)$ is interpreted as the reflection at junction (with continuity of section and slope) between a lossless cone and an anechoic lossy flared pipe (with constant curvature). In [24], a similar interpretation has been done for R_l^s and R_r^s in the case of lossless cones.

4) Interest of this framework: For acoustic reasons, the framework of Fig. 9 is interesting because the effects of the curvature and losses are isolated from the others (section and slope), and it makes their study easier. Because of the square roots of the function Γ (cf. (7)), the study requires special treatments (see sec. V-A).

For a systematic point of view, it is interesting to recover a symmetric general framework containing elementary cells of the *Kelly-Lochbaum* junction type. Moreover, as it is explained in sec. IV, this general framework makes possible to recover some former lossless waveguide models (cf. eg. [10], [11]), and some other lossy waveguide models by adding losses in propagation function $T(s)$ (cf. eg. [12], [14]). But in addition it takes into account both the curvature of the shape of pipe and the visco-thermal losses, according to the refined acoustic model of *Webster-Lokshin*.

IV. Network of pipes

In this section two-port systems of pieces of pipe are connected in order to build the model of a complete resonator. Using variables (p^+, p^-), it is necessary to study how the connection must be done.

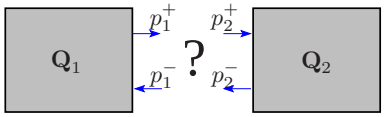

Fig. 10. Connecting 2 two-port with variables (p^+, p^-).

The right side of two-port $\mathbf{Q}_1$ is connected to left side of two-port $\mathbf{Q}_2$. The variables which are associated to $\mathbf{Q}_n$ for $n \in \{1, 2\}$, are named (p_n^+, p_n^-). Flow and pressure continuity assume that $P = p_1^+ + p_1^- = p_2^+ + p_2^-$ and $U = Y_c\left(p_1^+ - p_1^-\right) = Y_c\left(p_2^+ - p_2^-\right)$, which leads to:

$$p_1^+ = p_2^+ \quad \text{and} \quad p_1^- = p_2^-.$$

In consequence, the connection of 2 two-ports with variables (p^+, p^-) is made by branching the output of $\mathbf{Q}_1$ (p_1^+) to input of $\mathbf{Q}_2$ (p_2^+), and reciprocally.

A. Junction of any pieces of pipe

Using the framework of Fig. 9, it is possible to model, and then to simulate, the connection of two pieces of pipe, $\mathbf{Q}_1$ and $\mathbf{Q}_2$, with discontinuities of section, slope, curvature (and losses). The resulting two-port, $\mathcal{Q}_j^{1,2}$, of such a **j**unction is the connection of six cells, that is: $\mathcal{Q}_j^{1,2} \equiv \mathcal{Q}_{cl}^{r,1} \odot \mathcal{Q}_s^{r,1} \odot \mathcal{Q}_a^{r,1} \odot \mathcal{Q}_a^{l,2} \odot \mathcal{Q}_s^{l,2} \odot \mathcal{Q}_{cl}^{l,2}$.

With hypothesis on the order of discontinuity and on the shape of the pipe, this framework enables to recover some former waveguide models of the literature, using simplifications.

B. Junction of cylinders

Two lossless cylinders are considered. two-ports $\mathbf{Q}_1$ and $\mathbf{Q}_2$ represent them, with section area $\mathrm{A}_{1,r}$ and $\mathrm{A}_{2,l}$.

For lossless cylinders, cells $\mathcal{Q}_s$ and $\mathcal{Q}_{cl}$ are identity systems and only cells $\mathcal{Q}_a$ are present. The resulting two-port of such a **j**unction is the connection $\mathcal{Q}_{j,a}^{1,2} \equiv \mathcal{Q}_a^{r,1} \odot \mathcal{Q}_a^{l,2}$. This junction is presented on top of Fig. 11.

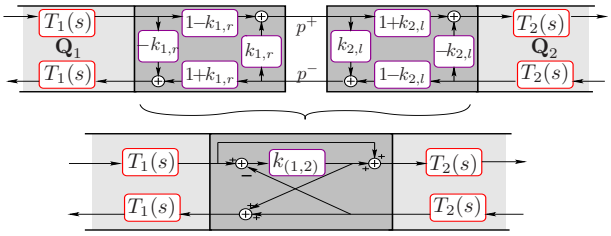

Fig. 11. Junction of lossless cylinders (with $T_i(s) = \mathrm{e}^{-s\tau_i}$)

Merging two-ports at interface leads to an equivalent two-port which represents the junction of cylinders (cf. bottom of Fig. 11). Using the algebraic laws of interconnections (cf. appendix A) and the expressions of $k_{1,r}$ and $k_{2,l}$ (cf. sec. III-B3 §1), the coefficient of reflexion is given by

$$k_{(1,2)} = \frac{\mathrm{A}_{1,r} - \mathrm{A}_{2,l}}{\mathrm{A}_{1,r} + \mathrm{A}_{2,l}}. \tag{34}$$

The *Kelly-Lochbaum* framework for networks of lossless cylinders is recovered (see eg. [10]). This model corresponds to the 0-*order* of discontinuity.

Remark that variables p^+ and p^- have now disappeared after merging, and $k_{(1,2)}$ does not depend on Z_c.

C. Junction of cones

Consider two lossless cones represented by two-ports $\mathbf{Q}_1$ and $\mathbf{Q}_2$, with slopes $r'_{1,r}$ and $r'_{2,l}$, connected with continuity of section.

The continuity of section (or radius) implies $r_{1,r} = r_{2,l} = r_j$ and $k_{(1,2)} = 0$. And for lossless cones, cells $\mathcal{Q}_{cl}$ are identity systems. Consequently, only the effect of difference of slopes remains. The resulting two-port of such a **j**unction is the connection $\mathcal{Q}_{j,s}^{1,2} \equiv \mathcal{Q}_s^{r,1} \odot \mathcal{Q}_s^{l,2}$ (see Fig. 12) where

$$R^s_{(1,2)}(s) = \frac{\alpha_{(1,2)}}{s - \alpha_{(1,2)}}, \tag{35}$$

$$\text{with} \qquad \alpha_{(1,2)} = \alpha_{1,r} + \alpha_{2,l} = +\tfrac{c_0}{2}\left(\frac{r'_{1,r} - r'_{2,l}}{r_j}\right). \tag{36}$$

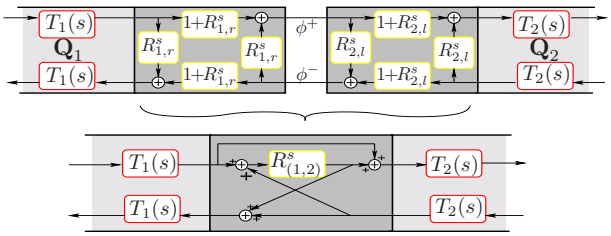

Fig. 12. Junction of lossless cones (with $T_i(s) = \mathrm{e}^{-s\tau_i}$)

The *Kelly-Lochbaum* framework is recovered for networks of lossless cones (see eg. [11]). It corresponds to the 1-*order* of discontinuity, with $\mathcal{C}^0$-regularity of the shape of pipe.

Remark: In [12], [14] the damping due to visco-thermal losses in propagation operators is taken into account, up to the same order of approximation ε (with $\Upsilon = 0$) of the acoustic model: $T(s) = \mathrm{e}^{-s\tau}\breve{D}(s)$ where

$$\breve{D}(s) := \mathrm{e}^{-\varepsilon\sqrt{s/c_0}L}. \tag{37}$$

D. Junction of constant-curvature pipe

Now a junction is considered with continuity of section ($\mathrm{A}_{1,r} = \mathrm{A}_{2,l}$) and continuity of slope ($r'_{1,r} = r'_{2,l}$), and two lossy flared pipes with different parameters are connected ($\Upsilon_1 \neq \Upsilon_2$ or $\varepsilon_1 \neq \varepsilon_2$).

$\mathcal{C}^1$-regularity implies $k_{(1,2)} = 0$ and $R^s_{(1,2)} = 0$. The resulting two-port of such a **j**unction is the connection $\mathcal{Q}_{j,cl}^{1,2} \equiv \mathcal{Q}_{cl}^{r,1} \odot \mathcal{Q}_{cl}^{l,2}$. This junction is presented in Fig. 13, where

$$R_{(1,2)}(s) = \frac{\Gamma_1(s) - \Gamma_2(s)}{\Gamma_1(s) + \Gamma_2(s)}, \tag{38}$$

$$\text{with} \quad \Gamma_n(s) = \sqrt{\left(\tfrac{s}{c_0}\right)^2 + 2\varepsilon_n\left(\tfrac{s}{c_0}\right)^{\frac{3}{2}} + \Upsilon_n}, \ \forall n \in \{1,2\}. \tag{39}$$

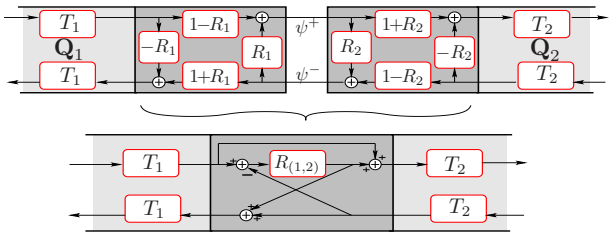

Fig. 13. Junction of lossy flared pipes with constant curvature (where $T_i(s) = \mathrm{e}^{-\Gamma_i(s)L_i}$).

The framework of *Kelly-Lochbaum* for networks of flared pipes with constant curvature is recovered (see [17]).

By comparing with former waveguide models, the improvement of this new model is that it allows junctions with continuity of section and slope, that is it can take into account the 2-*order* of discontinuity, with $r(\ell)$ $\mathcal{C}^1$-regular.

The analytical model of a network of some pieces of pipe with constant curvature per piece and with continuity of section and slope at junctions is proved to be stable. This proof is done by analyzing stability and passivity for one two-port of piece of pipe. Then by induction reasoning, the passivity of the connexion of a two-port of piece of pipe with any passive system, leads to the passivity and the stability of the whole network. No details are given in the present paper, but a next article will be devoted to this proof.

V. Digital waveguides and simulation

A. Diffusive representation, approximation and digital derivation

Because of the square roots in $\Gamma(s)$, some involved transfer functions are irrational, and so they are not standard. These transfer functions have continuous lines of singularities in $\mathbb{C}$,

which are named *cuts*. These cuts join some points (*branching points*) and the infinity.

If $\Upsilon = 0$, the function Γ has one branching point at $s = 0$. The cut $\mathbb{R}^-$ is chosen to preserve hermitian symmetry. Thereof, associated transfer functions have a continuous line of singularities on $\mathbb{R}^-$. Using the residue theorem, it has been shown (cf. eg. [25], [26], [27], [28]) that these functions are represented by a class of infinite-dimensional systems: *Diffusive Representations*. For any diffusive representation $H(s)$, analytic on $\mathbb{C}\backslash\mathbb{R}^-$:

$$H(s) = \int_0^\infty \frac{\mu_H(\xi)}{s+\xi} \mathrm{d}\xi, \tag{40}$$

$$\mu_H(\xi) = \frac{1}{2i\pi}\Big(H(-\xi+i0^-) - H(-\xi+i0^+)\Big). \tag{41}$$

For simulation in the time domain, in [29] for example, it has been proposed to approximate such diffusive representations by finite-dimensional approximations, given by $\widetilde{H}(s) = \sum_{j=1}^{j=J} \frac{\mu_j}{s+\xi_j}$, where J is the number of poles, $-\xi_j \in \mathbb{R}^-$ is the position of the jth pole and μ_j is its weight.

The poles are placed in $\mathbb{R}^-$ with a logarithmic scale, and the weights μ_j are obtained by a least-square optimization in the Fourier domain.

If $\Upsilon > 0$, Γ has two more branching points, which are complex conjugate. In this case, the diffusive representations are approximated with a finite sum of first and second order differential systems:

$$\widetilde{H}(s) = \sum_{j=1}^{j=J} \frac{\mu_j}{s+\xi_j} + \sum_{n=1}^{n=N} \left(\frac{w_n}{s+\gamma_n} + \frac{\overline{w}_n}{s+\overline{\gamma}_n} \right). \tag{42}$$

Transfer functions to approximate are: R_k, $R_{(k,k-1)}$ and D_k, for any k (see sections III-B3 (§4) and IV-D)[1]. Note that in models of [12] and [14], the transfer function $\breve{D}(s) = \mathrm{e}^{-\varepsilon_k \sqrt{s/\mathrm{c}_0} L_k}$ has to be approximated with poles on $\mathbb{R}^-$.

Finally, a digital version of (42) is implemented using standard numerical approximations (see [30], [31], [9]).

B. Numerical comparisons of three simulations

In this section, digital waveguide simulations of a *goal* pipe $\mathcal{P}_{goal}$ defined in sec. V-B1 are built approximating $\mathcal{P}_{goal}$ by straight (M1), conical (M2) or constant-curvature (M3) pieces of pipe. The sampling frequency F_s or length L are adapted so that no fractional delays are required. The number of pieces of pipe is chosen such that artefacts due to the discontinuities of the approximated shapes are rejected (see V-B2). The input impedances respectively obtained from (M1,M2,M3) are compared in the Fourier domain to the *goal* one (see V-B3).

Note that the three acoustic models take into account losses and the varying cross-section. By fixing an equivalent global complexity, the comparison is about the quality of approximations of the diffusive representations (cf. sec. V-A).

[1]The order of approximation $(J + 2N)$ depends on the desired quality: J mainly tunes the quality of approximation of effects due to visco-thermal losses, and N, that due to the curvature. For example, in the case of very large tubes, visco-thermal losses are negligible so that, the choice $J = 0$ can be done. Increasing J and N improves the approximation, and so the quality of the simulation, and decreasing J and N reduces the quality. In practice, choosing $J = 6$ and $N = 5$ leads to fully satisfactory results, in most cases (which corresponds to a 16^{th} order filter).

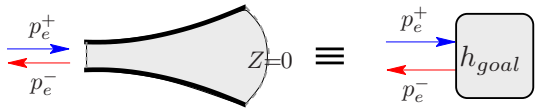

Fig. 14. The impulse response h_{goal} is the reflexion of the virtual pipe.

1) Goal pipe, lengths and sampling frequencies: The *goal* pipe is defined by $r(\ell) = R_0 + \ell^\alpha$ on $\ell \in [0, L]$, with $R_0 = 2.5$ mm and $\alpha = 4$. This pipe is terminated at the right end by a zero impedance. Here, only digital simulation of acoustic tubes is studied, and the *goal* pipe is ideally open in order not to introduce a model of sound radiation.

The exact impulse response of the global reflexion function of the *goal* pipe is denoted $h_{goal}(t)$ (see Fig. 14). Moreover, the input impedance $Z_{goal}(i\omega)$ is computed for each ω as follows: [step 1] for each (fixed) $s = i\omega$, numerically solve the linear Cauchy problem (1), (2) on $\ell \in [0, L]$ with the boundary condition $P(\ell = L, s) = 0$, $U(\ell = L, s) = 1$; [step 2] compute

$$Z_{goal}(s) = \frac{P(0,s)}{U(0,s)} = -\frac{\rho_0\, s}{\mathrm{A}_0} \times \frac{P(\ell=0,s)}{\partial_\ell P(\ell=0,s)}, \tag{43}$$

with $s = i\omega$. Results are presented in Fig. 15 (curve C0).

For simulations based on (M3) which relies on the curvilinear length ℓ, the following choice is made to have no fractional delays: $F_s = 44100\,\mathrm{Hz}$ and $L = K\,\mathrm{c}_0\,/F_s \approx 49.9\,\mathrm{cm}$ with $K = 64$. From (3), the corresponding axial length is $L_z = \ell^{-1}(L) \approx 49.0\,\mathrm{cm}$ so that the corresponding sampling rate is $F_z = K\,\mathrm{c}_0\,/L_z \approx 44924\,\mathrm{Hz}$ for (M1).

2) Number of pieces of pipe for models (M1, M2, M3): First, for (M1) with $\varepsilon = 0$, the continuous-time impulse response associated to pieces of pipe with length δz_1 writes

$$h_1(t) = \sum_{n=0}^{+\infty} a_n \delta(t - 2n\,\delta z_1/\,\mathrm{c}_0) \tag{44}$$

where $\delta(.)$ denotes the Dirac distribution, and the a_n's can be deduced from reflexion coefficients k in (34). Hence, the choice $\delta z_1 = \mathrm{c}_0\,/(2F_z)$ yields the digitalized impulse response $h(t_n) = a_n$ which avoids discontinuities due to the artificial intertwined "zeros" naturally involved by (M1). According to this well-known and standard result, the number of pieces of pipe is then chosen as $2K = 128$. Note that for $\varepsilon > 0$, (44) becomes smoother since the losses introduce dissipation through $\breve{D}$ in (37) which corresponds to the slowly decreasing impulse response (cf. [32]) $\tilde{d}(t) = (\beta/(2\sqrt{\pi t^3}))\,\mathrm{e}^{-\beta^2/(4t)}$ for $t > 0$ with $\beta = \varepsilon\,\delta z_1/\sqrt{\mathrm{c}_0}$. But, this regularization is not sufficient to decrease the number $2K$ (see Fig. 23-(1,2,3) p.14).

Second, for (M2) with $\epsilon = 0$, the corresponding continuous-time impulse response h_2 involves decreasing exponentials (cf. [24], [33]) and digital versions involve first order filters so that the computational cost for one piece of pipe is twice greater for cones than for cylinders. To preserve a similar global computational cost and since the discontinuity of h_2 is smoothed by exponential responses, the number of pieces of pipe is chosen as $K = 64$ so that $\delta z_2 = 2\delta z_1$. In practice, this actually yields smooth results (see Fig. 23-(4,5,6) p.14).

Third, (M3) leads to a naturally smooth impulse response h_3 and reducing the number of pieces of pipe does not introduce artefacts of discontinuity type but only influences the quality of approximation. In practice, taking only 4 pieces of pipe with constant curvature yields accurate results (see Fig. 23-(7)).

3) Digital waveguides, input impedances and comparisons: Each digital simulation based on (M1,M2,M3) is built with a Kelly-Lochbaum framework derived as in sections IV-B to IV-D. In these networks, time domain versions of $T_i(s)$ (see (15), (16) and (37)) are implemented using a circular buffer for the delay part and using recursive digital filters straightforwardly deduced from optimisations of $D_i(s)$ and $\breve{D}_i(s)$ following the method presented in sec. V-A. Digital filters are also obtained for $R^s_{i,i+1}$, $R_{i,i+1}$ in the same way.

From the number of floatting point operations and the CPU point of view, parameters J, N involved in the approximations (42) of the diffusive representations are chosen in order to preserve the same algorithmic complexity. Then, the ξ_j's and γ_n are optimized to have the best results following the method proposed in [29].

In practice, the simulation network for (M1) involves $2K = 128$ delays and reflexion coefficients $k_{i,i+1}$, and $\breve{D}_i$ are approximated using second order filters. The network for (M2) involves $K = 64$ circular buffers for delays, 64 first order filters for reflexions $R^s_{i,i+1}$ and 64 fourth order filters for approximating $\breve{D}_i$. Finally, the network for (M3) involves 4 pieces of pipe: 8 circular buffers, 8 filters for approximating D_i, 5 filters for approximating $R_{i,i+1}$ with distinct orders but leading to the same global complexity as previous models (which are "globally" equivalent to 170^{th} order filters).

The input impedances corresponding to (M1,M2,M3) are respectively deduced from the discrete-time Fourier transforms R_1^{glob}, R_2^{glob}, R_3^{glob} of the digital impulse responses h_1, h_2 and h_3 of the global input reflexion (similar to Fig. 14) using

$$\underline{Z}_{in}(f) = \frac{Z_c \pi R_0^2}{\rho_0\, c_0} \times \frac{1 + R_{glob}(f)}{1 - R_{glob}(f)} \qquad (45)$$

where f denotes the frequency.

These impedances and the *goal* impedance are plotted in Fig. 15. To help comparisons, their spectral envelopes which links local maxima are also plotted. Frequency positions of maxima coincide for all models (with an error ± 15 Hz), but not their amplitude. More precisely, for (M1) and (M2), amplitudes are significantly too high between 0 and 3000 Hz and too small in $[4000, 6000]$ Hz. On the contrary, model (M3) better fits with the *goal* impedance with an accuracy smaller than 2 dB.

The reason is that many pieces of pipe are required (128 for (M1), 64 for (M2)), so to respect the given "global" algorithmic complexity only low order filters can be used to approximate the $\breve{D}$'s which account for losses. On the contrary, with only 4 pieces of pipe, (M3) allows higher orders for approximations together with an equivalent global complexity and a best quality. Moreover, it is possible to adjust complexity and quality, by adapting the values of J and N for each approximation (cf. sec. V-A).

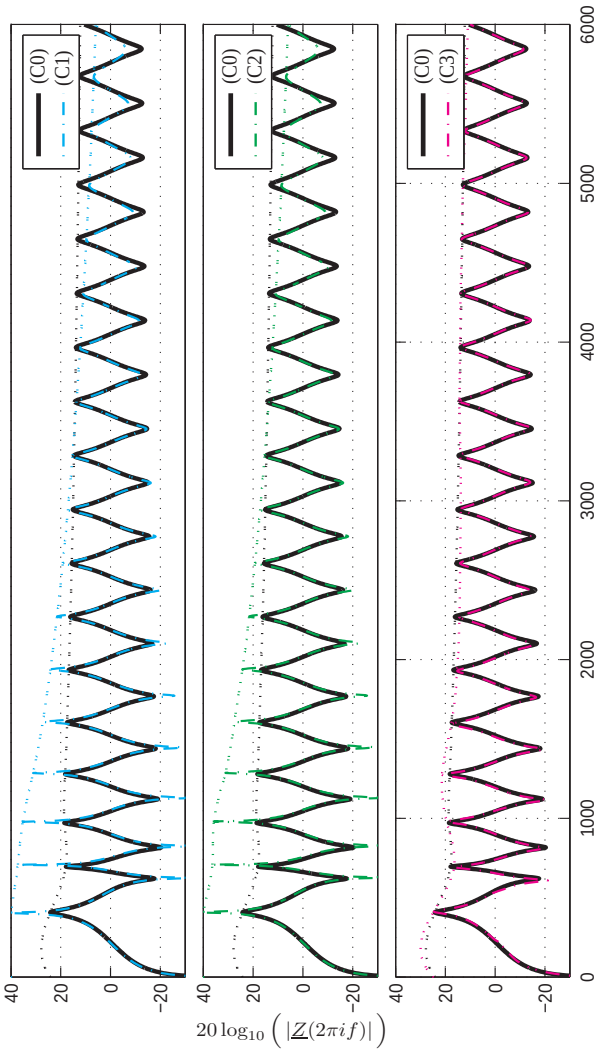

Fig. 15. Comparisons between the *goal* impedance Z_{goal} and impedances obtained from (M1), (M2) and (M3). Curve (C0) is the impedance Z_{goal}. It is numerically computed using a standard Runge-Kutta method (cf. [34]) (Matlab©: ode23 with a relative error $\delta = 10^{-3}$). Curves (C1,C2,C3) are deduced from the simulation of 128 cylinders, of 64 cones and of 4 constant-curvature pipes, respectively. Dotted curves represent envelopes of maxima.

C. Building a virtual instrument

This section deals with the resonator of a virtual trombone modeled by concatenating seven elements (see Fig. 16, top): a mouth-piece, five pieces of pipe (1 cylinder and 4 flared pipes with constant curvature), and a radiation impedance.

The mouthpiece is modeled by an acoustic mass (cf. [35]), a resistance, and a compliance, and it is simulated by a second order system. Because of the flaring at the end of the horn of brass instruments, the radiation model of [36] seems well adapted for this application; here this model is used. The cylinder models the slide of the trombone and the four flared pieces of pipe model the horn. Parameters (lengths and curvatures) of these pieces of pipe have been empirically tuned such that the approximated shape fits the radius measured on a real trombone (see appendix B for details). The measurements correspond to a Courtois trombone.

Note that, with $r_{min} \approx 7$ mm and $r_{max} \approx 11$ cm (the

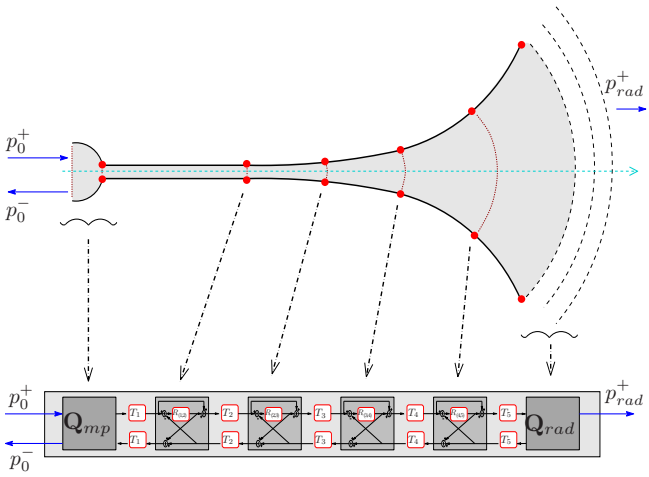

Fig. 16. Making a virtual trombone

extreme radii), the *Webster-Lokshin* model is valid at least with $0.13 \ll f < 915$ Hz (for validation of losses and longitunal propagation). For trombones, this limitation is satisfactory considering that the coupling of the resonator and the excitator (the lips, cf. eg. [37]), mainly involves lower modes.

The approximated shape is $\mathcal{C}^1$-regular, and so the *Kelly-Lochbaum* framework is recovered for the whole pipe of the trombone, leading to Fig. 16 (bottom). Figure 18 compares the impedance measured on the real trombone to that computed from the digital time simulation of the impulse response.

Figure 18 shows that the modelisation is globally correct, but with some significant errors in the spectral envelop around 300 and 600 Hz. This difference comes from the rough empirical approximation of the original profil. Nevertheless, some recent works will allow better automatic approximations of the profile (cf. [38]).

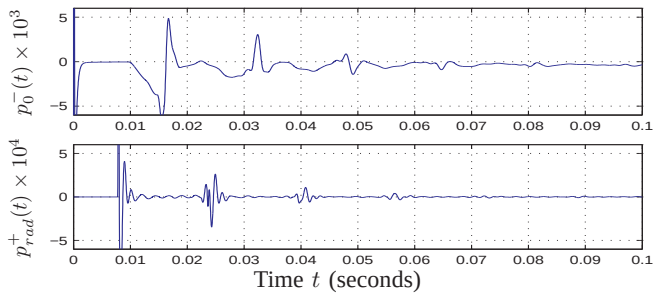

Fig. 17. Input (top) and output (bottom) impulse responses (digital time simulation).

VI. Conclusions and perspectives

In this paper, the *Webster-Lokshin* model has been used to build digital waveguides taking into account both visco-thermal losses at the wall, and curvature of the shape of pipe.

A "generalized" framework has been derived in which delays and effects due to the shape are separated (section, slope and curvature). Considering particular cases of regularity at junctions of pieces of pipe, three kinds of Kelly-Lochbaum networks are recovered. One of them makes it possible to

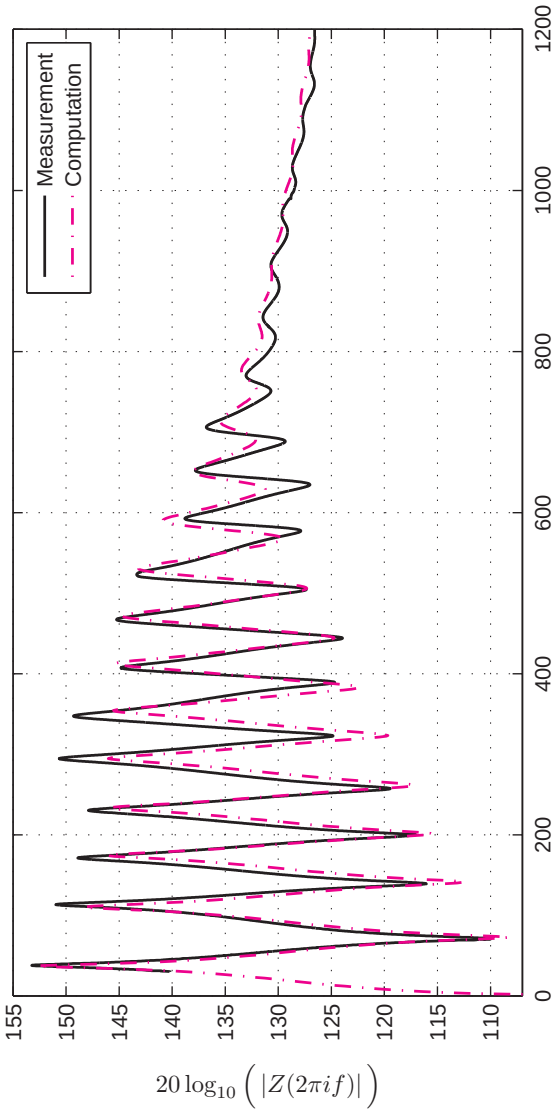

Fig. 18. Measured and computed impedances.

consider junctions with continuity of section and slope, and discontinuity of curvature, which means the $\mathcal{C}^1$-regularity of the shape.

Moreover, this model does not impose a number of pieces of pipe, contrarily to models of connections of straight and conical pieces of pipe. In sec. V-B, whereas 128 cylinders (M1) or 64 cones (M2) are required to model the *goal* pipe, 4 constant curvature pieces of pipe are enough to get good results (M3). Using this improvement, digital real-time simulations has been implemented in C/C++ language.

In the particular case of $\mathcal{C}^1$-regularity (with $\Upsilon(\ell) > 0$), the stability and passivity of transfer functions involved in the global Kelly-Lochbaum network can be proved analytically (in the Laplace domain). This specific aspect of the work will be presented in a future paper.

However, for negative curvatures, some transfer functions involved in the Kelly-Lochbaum network are unstable. This phenomenon is quite complicated, but is now well understood (see eg. [7]). Very similar phenomena appear at junctions of cones, when the difference of slopes (on both size of

the junction) is negative (cf. [24], [14]). In [39], the simple case of a single convergent cone has been studied, and the corresponding Kelly-Lochbaum network has been proved to be internally stable if it is represented by its minimal realization, in the sense of the state-space representations of systems. Hence, an approach to cope with the problem of negative curvature could be based on an extension of solutions which have been proposed for networks of cones.

In this paper, the example of a virtual trombone is presented to illustrate some results of simulations. The application of the presented model to the simulation of the vocal tract will be considered after solving the problem of negative curvatures.

Appendix A
Connecting 2 two-ports

Connecting 2 two-ports consists in branching output of one two-port to input of the other, and reciprocally as top of Fig. 19 shows.

Merging these two-ports into a unique equivalent two-port is interesting for some reasons:

- First, in some cases, the merging allows to simplify the framework.
- It can be used to prove the equivalence between some different forms of a two-port system.
- As Fig. 19 shows, there is an instantaneous loop at interface which cannot be simulated numerically.

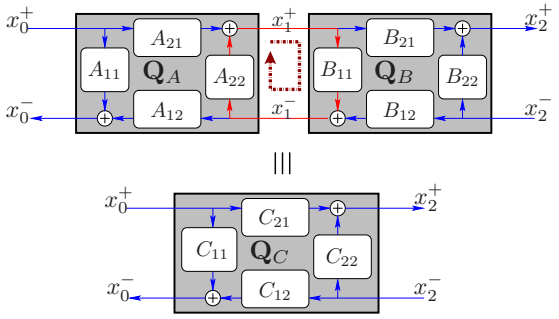

Fig. 19. Connecting two-ports and removing instantaneous loops

In Fig. 19, $\mathbf{Q}_C$ is defined as the equivalent two-port of the connection of two-ports $\mathbf{Q}_A$ and $\mathbf{Q}_B$. In [22], the following notation is defined: $\mathbf{Q}_C \equiv \mathbf{Q}_A \odot \mathbf{Q}_B$, where $\equiv$ is the equivalent relation and $\odot$ is the connection operator.

Algebraic expressions of elements of $\mathbf{Q}_C$ are

$$C_{11} = A_{11} + \frac{A_{12}B_{11}A_{21}}{1 - A_{22}B_{11}}, \quad (46)$$

$$C_{12} = \frac{B_{12}A_{12}}{1 - A_{22}B_{11}}, \quad (47)$$

$$C_{21} = \frac{A_{21}B_{21}}{1 - A_{22}B_{11}}, \quad (48)$$

$$C_{22} = B_{22} + \frac{B_{12}A_{22}B_{21}}{1 - A_{22}B_{11}}, \quad (49)$$

for which $A_{22}(s)B_{11}(s) \neq 1$, $\forall s / \Re e(s) > 0$ is required to guarantee the stability of the feedback loop.

Appendix B
Table of parameters of section V-C

In the following table, the subscript c means the *cup* of the mouth-piece of the trombone and b means its *backbore*. r_c and V_c are the radius and the volume of the cup, L_b and r_b are the length and the equivalent radius of the backbore. C_a is the acoustic compliance of the cup, R_a and M_a are the acoustic resistance and the acoustic mass associated to the backbore (see [35]).

Mouthpiece parameters:

r_c (m)	V_c (m^3)	L_b (m)	r_b (m)
$14.5\ 10^{-3}$	$10.8\ 10^{-6}$	$52.5\ 10^{-3}$	$4.5\ 10^{-3}$
$C_a(m^3.P_a^{-1})$	$M_a(kg.m^{-4})$	$R_a(N.s.m^{-5})$	
$7.59\ 10^{-11}$	990	$5.87\ 10^{-3}$	

Pieces of pipe parameters:

Number	1	2	3	4	5
r_l (mm)	6.9	6.9	10.4	22	43.7
r_r (mm)	6.9	10.4	22	43.7	110
r'_l	0	0	0.013	0.055	0.5
r'_r	0	0.013	0.055	0.5	0.99
L (m)	1.615	0.544	0.352	0.103	0.085
Υ (m^{-2})	0	3	9	120	60
ε $(m^{-\frac{1}{2}})$	0.0507	0.0422	0.0248	0.0116	0.0033

Note that, parameters $C_a, R_a, M_a, r'_l, r'_r$ and ε are calculated from the others. For constant curvature, $\varepsilon(\ell)$ varies with $r(\ell)$, ε is chosen as the mean of $\varepsilon(\ell)$ along the piece of pipe.

Appendix C
Effects of curvature and losses on Webster-Lokshin transfer functions

The input impedance of a cylinder which is ideally open at right (that is $P_L = 0$) is drawn in Fig. 20 for various loss coefficients: $\varepsilon = 0$ (no losses), $\varepsilon = \varepsilon^*$ computed from the standard physical values, and $\varepsilon = 3\,\varepsilon^*$ (artificially overestimated losses).

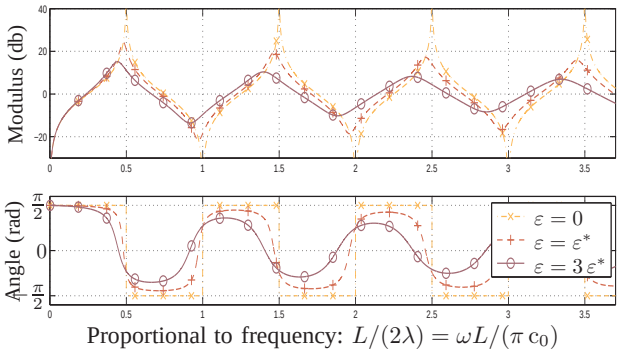

Fig. 20. Influence of losses on the impedance of an open cylinder, H_{11}^{-1}. Parameters: $r_0 = r_L = 5mm, L = 1m, \Upsilon = 0m^{-2}$.

Figure 21 compares the effects of the curvature value on the input impedance $Z_{in} = 1/H_{11}$ of an ideally open pipe (see also Fig. 1). Vertical dashed lines represent the cutoff frequency ω_c for each curvature.

Figure 22 compares the effects of the curvature value on the input impedance $Z_{in} = 1/H_{11}^l$ of a semi-infinite pipe (see also

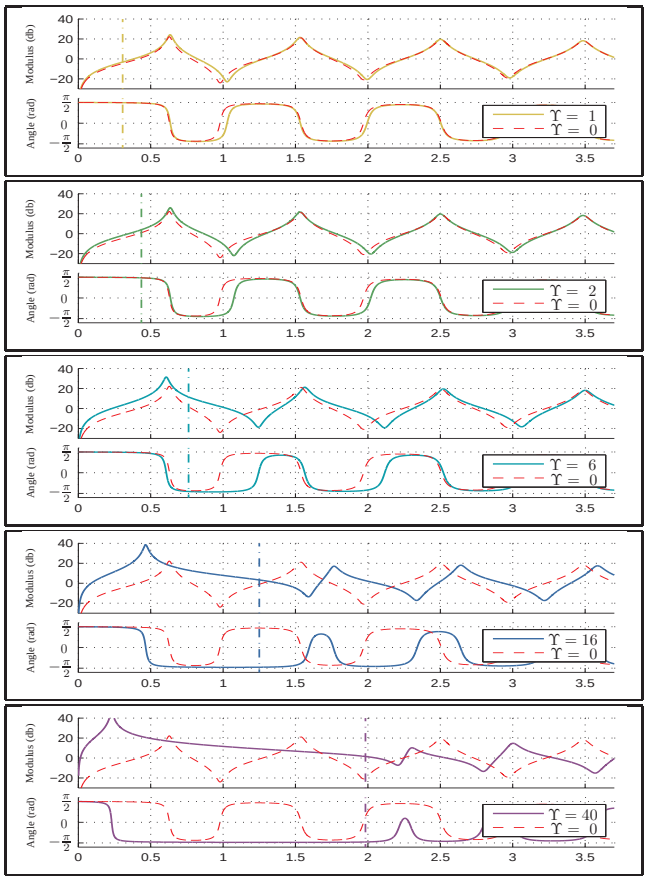

Fig. 21. Influence of the curvature on the impedance of an open pipe, H_{11}^{-1}. Parameters: $r_0 = 5$ mm, $r_L = 10$ mm, $L = 1$ m. Abscissa: kL/π.

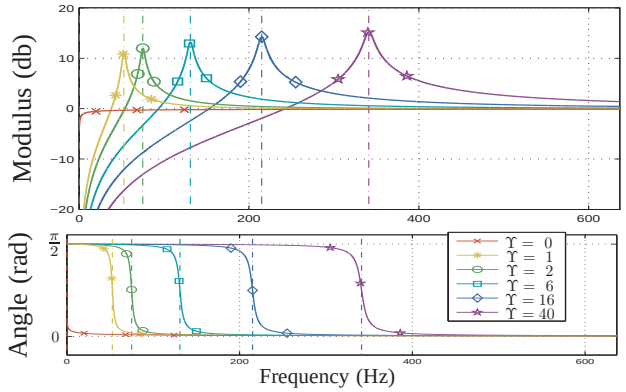

Fig. 22. Influence of the curvature on the impedance of a semi-infinite pipe, $G_{11}^{l}(s = 2i\pi f)$. Parameters: $r_l = 5$ mm, $\varepsilon = 0.0525$ m$^{-\frac{1}{2}}$, $\zeta_l = 0$ m^{-1}.

Fig. 7). Vertical dashed lines represent the cutoff frequency for each curvature.

REFERENCES

[1] J. O. Smith, "Physical modeling synthesis update," *Computer Music Journal*, vol. 20, no. 2, pp. 44–56, 1996, MIT Press.

[2] S. Bilbao, *Waves and Scattering Methods for Numerical Simulation*. Chichester: John Wiley and Sons, 2004.

[3] A. A. Lokshin and V. E. Rok, "Fundamental solutions of the wave equation with retarded time," *Dokl. Akad. Nauk SSSR*, vol. 239, pp. 1305–1308, 1978, (in Russian).

[4] A. A. Lokshin, "Wave equation with singular retarded time," *Dokl. Akad. Nauk SSSR*, vol. 240, pp. 43–46, 1978, (in Russian).

[5] J.-D. Polack, "Time domain solution of Kirchhoff's equation for sound propagation in viscothermal gases: a diffusion process," *J. Acoustique*, vol. 4, pp. 47–67, Feb. 1991.

[6] A. Webster, "Acoustic impedance and the theory of horns and of the phonograph," *Proc. Nat. Acad. Sci. U.S*, vol. 5, 1919.

[7] D. P. Berners, "Acoustics and signal processing techniques for physical modeling of brass instruments," Ph.D. dissertation, Standford University, 1999.

[8] T. Hélie, "Unidimensional models of acoustic propagation in axisymmetric waveguides," *J. Acoust. Soc. Am.*, vol. 114, pp. 2633–2647, 2003.

[9] T. Hélie and D. Matignon, "Diffusive reprentations for the analysis and simulation of flared acoustic pipes with visco-thermal losses," *Mathematical Models and Methods in Applied Sciences*, vol. 16, pp. 503–536, Jan. 2006.

[10] J. D. Markel and A. H. Gray, *Linear Prediction of speech*. Berlin: Springer-Verlag, 1976.

[11] V. Välimäki, "Discrete-time modeling of acoustic tubes using fractional delay filters," Ph.D. dissertation, Helsinki University of Technology, 1995.

[12] D. Matignon and B. d'Andréa-Novel, "Spectral and time-domain consequences of an integro-differential perturbation of the wave PDE," in *WAVES'95*. Mandelieu, France: INRIA, SIAM, April 1995, pp. 769–771.

[13] D. Matignon, "Représentations en variables d'état de guides d'ondes avec dérivation fractionnaire (state space representation of waveguides with fractional derivative)," Ph.D. dissertation, Université Paris-Sud, 1994.

[14] E. Ducasse, "An alternative to the traveling-wave approach for use in two-port descriptions of acoustic bores," *J. Acoust. Soc. Am.*, vol. 112, pp. 3031–3041, 2002.

[15] ——, "Modélisation et simulation dans le domaine temporel d'instruments à vent à anche simple en situation de jeu: méthodes et modèles (modeling and simulation in the time domain of reed instruments in playing situation: methods and models)," Ph.D. dissertation, Université du Maine, 2001.

[16] M. V. Walstijn, "Discrete-time modelling of brass and reed woodwind instruments with application to musical sound synthesis," Ph.D. dissertation, University of Edinburgh, 2002.

[17] T. Hélie, R. Mignot, and D. Matignon, "Waveguide modeling of lossy flared acoustic pipes: derivation of a Kelly-Lochbaum structure for real-time simulations," in *IEEE WASPAA*, Mohonk, USA, 2007, pp. 267–270.

[18] G. P. Scavone, "An acoustic analysis of single-reed woodwind instruments with an emphasis on design and performance issues and digital waveguide modeling techniques," Ph.D. dissertation, Music Dept., Stanford University, 1997.

[19] T. Hélie, "Modélisation physique des instruments de musique en systêmes dynamiques et inversion (physical modeling of musical instruments by dynamical system and inversion)," Ph.D. dissertation, Université Paris-Sud, Orsay, France, 2002.

[20] M. Bruneau, *Manuel d'acoustique fondamentale*. Paris: Hermès, 1998.

[21] J. Kemp, "Theoretical and experimental study of wave propagation in brass musical instruments," Ph.D. dissertation, University of Edinburgh, 2002.

[22] P. Depalle and S. Tassart, "State space sound synthesis and a state space synthesiser builder," in *Int. Computer Music Conf. (ICMC'95)*. Computer Music Association, Sept. 1995, pp. 88–95.

[23] R. Mignot, T. Hélie, and D. Matignon, "On the singularities of fractional differential systems, using a mathematical limiting process based on physical grounds," *Physica Scripta*, accepted for publication in 2009.

[24] J. Gilbert, J. Kergomard, and J.-D. Polack, "On the reflection functions associated with discontinuities in conical bores," *J. Acoust. Soc. Am.*, vol. 04, 1990.

[25] O. J. Staffans, "Well-posedness and stabilizability of a viscoealistic in energy space," *Trans. Amer. Math. Soc.*, vol. 345, no. 2, pp. 527–575, 1994.

[26] G. Montseny, "Diffusive representation of pseudo-differential time-operators," *ESAIM: Proc*, vol. 5, pp. 159–175, 1998.

[27] T. Hélie and D. Matignon, "Representation with poles and cuts for the time-domain simulation of fractional systems and irrational transfer functions," *Journal of Signal Processing, Special Issue on Fractional Calculus Applications in Signals and Systems*, vol. 86, pp. 2516–2528, 2006.

[28] D. Matignon, "Stability properties for generalized fractional differential systems," *ESAIM: Proc*, vol. 5, pp. 145–158, 1998.

[29] T. Helie, D. Matignon, and R. Mignot, "Criterion design for optimizing low-cost approximations of infinite-dimensional systems: Towards efficient real-time simulation," *Int. Journal of Tomography and Statistics*, pp. 13–18, 2007.

[30] T. W. Parks and C. S. Burrus, *Digital Filter Design*. New York: John Wiley and Sons, Inc., 1987.
[31] G. F. Franklin, J. D. Powell, and M. L. Workman, *Digital Control of Dynamic Systems*. Menlo-Park: Addison-Wesley, 1990, page 150.
[32] M. Abramowitz and I. A. Stegun, *Handbook of mathematical functions*. New York: Dover, 1970, eq.(29.3.82).
[33] A. Barjau, D. H. Keefe, and S. Cardona, "Time-domain simulation of acoustical waveguides with arbitrarily spaced discontinuities," *J. Acoust. Soc. Am.*, vol. 105, 1998.
[34] P. Bogacki and L. F. Shampine, "A 3(2) pair of Runge-Kutta formulas," *Appl. Math. Letters*, vol. 2, pp. 1–9, 1989.
[35] N. H. Fletcher and T. D. Rossing, *Physics of musical instruments*. New York: Springer Verlag, 1991.
[36] T. Hélie and X. Rodet, "Radiation of a pulsating portion of a sphere: application to horn radiation," *Acta Acustica*, vol. 89, pp. 565–577, 2003.
[37] C. Vergez and X. Rodet, "Experiments with an artificial mouth for trumpet," in *ISMA98*, Leavenworth, Washington State, USA, 1998.
[38] T. Hézard, T. Hélie, and R. Mignot, "Représentation géométrique optimale de la perce de cuivres pour le calcul d'impédance d'entrée et de transmittance, et pour l'aide à la lutherie," in *Congrès Français d'Acoustique (CFA10)*, Lyon, France, 2010. in publication.
[39] R. Mignot, T. Hélie, and D. Matignon, "Stable realization of a delay system modeling a convergent acoustic cone," in *Mediterranean Conference on Control and Automation*, vol. 16, Ajaccio, France, 2008, pp. 1574–1579.

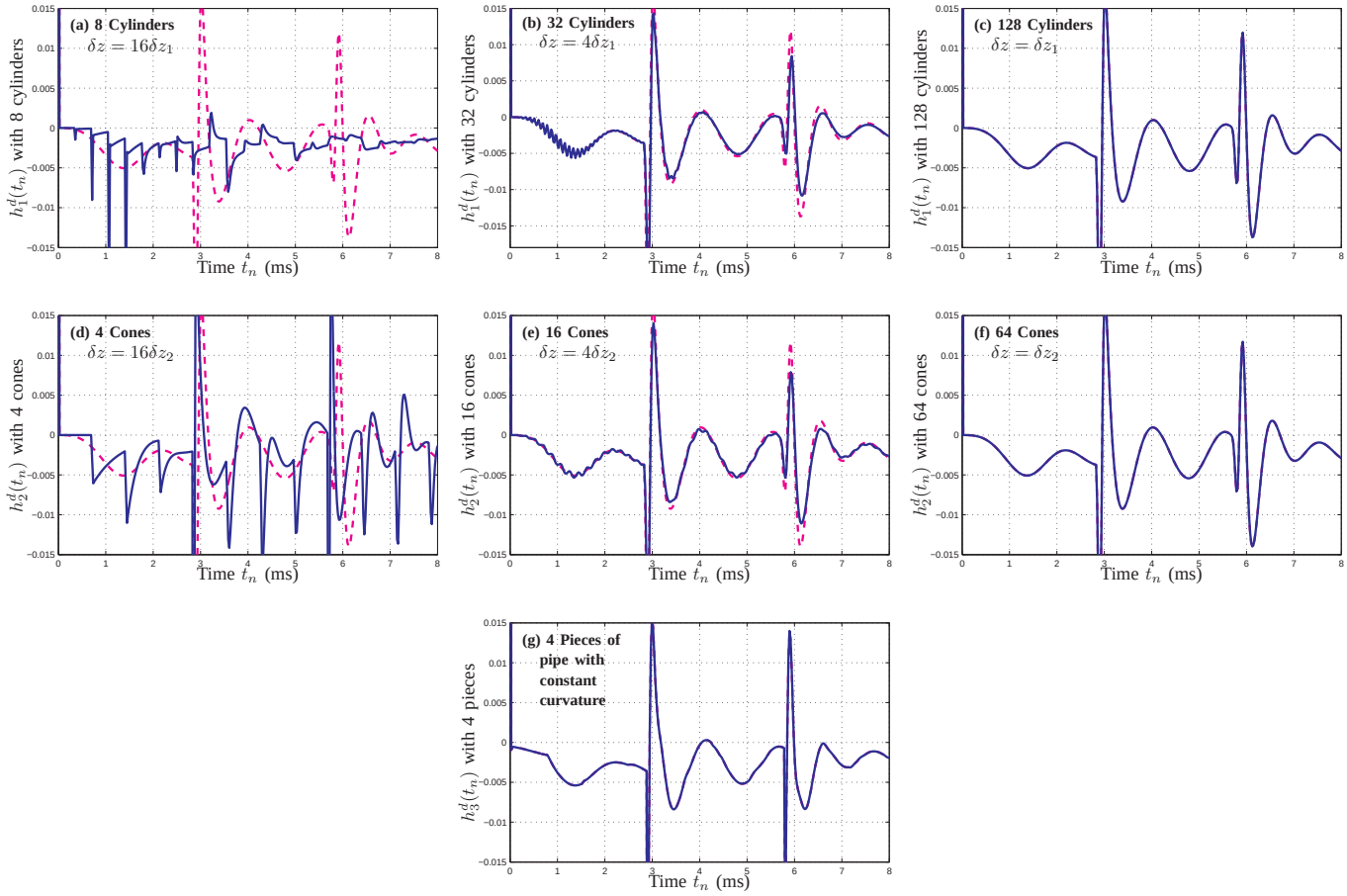

Fig. 23. Digital impulse responses of simulations in the discrete time domain (cf. sec. V-B2 p. 8): (a) Connection of 8 cylinders, (b) connection of 32 cylinders, (c) connection of 128 cylinders, (d) connection of 4 cones, (e) connection of 16 cones, (f) connection of 64 cones, (g) connection of 4 constant-curvature pipes. The dashed curves are the correctly sampled impulse responses for cylinders and cones.